

**7th International Conference
on
Wind Turbine Noise
Rotterdam – 2nd to 5th May 2017**

**Small Horizontal Axis Wind Turbine:
Aeroacoustic and Aerodynamic Optimization
of Airfoil Shape and Blade**

**K. Volkmer, N. Kaufmann, T. Carolus
University of Siegen, 57076 Siegen, Germany**

Corresponding author: kevin.volkmer@uni-siegen.de

Summary

Objective of this contribution is an acoustic and aerodynamic optimization of the full 3D blade geometry for a small horizontal axis wind turbine. Utilizing a refined aerodynamic blade element momentum (BEM) method and a combination of ROZENBERG's wall pressure and AMIET's trailing edge noise model an evolutionary algorithm is implemented. The validity of ROZENBERG and AMIET models was checked by comparison with recent own measurements of the wall pressure fluctuations and trailing edge sound of a small airfoil section. The optimization is subdivided into two independent steps, (i) the airfoil optimization, and (ii) the optimization of the blade twist angle and chord length distributions. To mimic a fully turbulent flow around the blades of a realistic wind turbine - a worst case scenario - tripping was applied close to the leading edge of all airfoils. The airfoil optimization resulted in novel airfoil shapes. As compared to a chosen benchmark airfoil S834 they promise a better lift-to-drag-ratio and/or lower non-dimensional wall pressure fluctuations in the trailing edge region (WPS). The predictions forecast a reduction by more than 10 dB. Utilizing such a low noise airfoil and optimizing spanwise chord length and twist angle distribution in a second step results in new blade designs. As compared to an existing, non-optimized research turbine with SOMERS airfoil shaped blades the predicted sound power of an optimized turbine is substantially lower without degradation of its power coefficient. A detailed analysis shows that the sound reduction is mainly attributed to the improved airfoil sections. Since the optimization and all results presented here are mainly based on models, future experimental validation is indispensable.

Nomenclature

Symbols

A	m^2	swept area of the turbine rotor
C	m	chord length
C_f	-	skin friction coefficient

C_D	-	drag coefficient
C_L	-	lift coefficient
C_P	-	power coefficient
D	-	Dimension
F	N	Force
H	-	boundary layer shape factor
I	-	radiation integral
K	rad/m	convective wavenumber
L	m	span
L_{Spp}	dB	level of power spectral density of far field acoustic pressure
$L_{\phi pp}$	dB	level of power spectral density of wall pressure
$LPBE$	dB	overall sound power level of a blade element
M	-	free stream Mach number
$OSPL$	dB	overall sound power level of whole wind turbine
P	W	power
$P_{\phi pp}$	-	power of the non-dimensional wall pressure fluctuations
PT	-	penalty term
R	m	total radius
Re	-	Reynolds number
Re_{θ}	-	Reynolds number based on θ and w_e
R_T	-	Ratio of outer to inner boundary layer timescale
S_0	m	corrected observer distance
S_P	W/Hz	sound power spectral density
S_{PP}	Pa ² /Hz	power spectral density of far field acoustic pressure
c_0	m/s	speed of incoming wind far upstream
c_s	m/s	speed of sound
f	Hz	frequency
f_{obj}	-	objective function
k	rad/m	acoustic wavenumber
l_y	m	spanwise correlation length
n	1/s	rotational speed
n_{BE}	-	number of blade elements
$n_{2D,PT}, n_{3D,PT}$	-	number of penalty terms in 2D and 3D
p	Pa	pressure
r	m	radius
u	m/s	circumferential velocity
w	m/s	relative velocity
$x_{1,2,3}$	m	Cartesian co-ordinates
z	-	number of blades

Greek symbols

Δ	-	ZAGAROLA-SMITS' parameter
----------	---	---------------------------

Φ_{pp}	Pa ² /rad	Power spectral density of surface pressure fluctuations
$\tilde{\Phi}_{pp}$	-	Normalized power spectral density of surface pressure fluctuations
Π	-	COLE's wake strength parameter
α	°	angle of attack
β	°	flow angle
β_c	-	CLAUSER's equilibrium parameter
γ	°	twist angle
δ	m	boundary layer thickness
δ^*	m	boundary layer displacement thickness
ε	-	lift-to-drag-ratio
κ	rad/m	frequency parameter
θ	m	boundary layer momentum thickness
λ	-	tip speed ratio
ν	m ² /s	kinematic viscosity
ρ	kg/m ³	air density
τ_{max}	Pa	maximum shear stress
τ_w	Pa	wall shear stress
ω	rad/s	angular frequency
$\tilde{\omega}$	-	Strouhal number based on external variables

Subscripts

0	position far upstream
∞	position in rotor plane
S_{pp}	power spectral density of far field acoustic pressure
e	position at boundary layer edge
obj	objective
ref	reference
sh	shaft
tip	at rotor tip
u	circumferential
w	weighing

Abbreviations

BE	blade element
BEM	blade element momentum theory
WPS	wall pressure spectra
WT	wind turbine

1. Introduction

Several criteria are relevant for designing the twisted, tapered and carefully profiled blades of horizontal axis wind turbines. Naturally, the maximum energy output of a wind turbine is of primary concern and achieved by optimal aerodynamic design. Yet, wind turbine industry is focusing on the analysis and mitigation of flow induced noise – on a par with efficiency, structural health, cost etc.

A classical semi-analytic blade design method is e.g. by GLAUERT and SCHMITZ, see for instance GASCH and TWELE [1]. Its outcome is a 3D blade, where the energy transferred to the shaft by each thought blade element of the segmented blade is theoretically maximal. However, the resulting spanwise geometry and aerodynamic loading distribution may not be optimal with respect to other criteria, e.g. flow induced noise.

A combined acoustic and aerodynamic optimization of the full 3D blade geometry is demanding. LELOUDAS [2] reported an optimization of twist and chord length distribution as well as the spatial distribution of given airfoil shapes, but excluded the optimization of the 2D airfoil shape itself. TIAN et al. [3] created an aeroacoustic prediction methodology for wind turbines by combining the aerodynamic airfoil performance prediction tool Xfoil (DRELA [4]), a model for wall pressure spectra (WPS) by ROZENBERG et al. [5], and AMIET's trailing edge noise model [6] with advanced models by ROGER and MOREAU [7]. In addition, AMIET's inflow turbulence noise model [8] was also implemented. Comparison to experimental data from isolated airfoil sections and a complete wind turbine were promising. In principle such a model could be used for optimization, but TIAN et al. did not elaborate on that.

Detailed aerodynamic and aeroacoustic airfoil shape optimization has been tried in the past. SCHEPERS et al. [9] and BERTAGNOLIO [10] utilized the TNO-model (named after the TNO Institute of Applied Physics, Netherlands) with simplified boundary layer characteristics as inputs. GÖCMEN and ÖZERDEM [11] utilized the Brooks-Pope-Marcolini (BPM) model [12] to implement an airfoil optimization tool.

A more integrated optimization, i.e. of twist and chord length distribution with respect to only aerodynamic performance and of airfoil shape with respect to aerodynamic and aeroacoustic performance, has been reported by HAO et al. [13]. Based on the simple BPM model, RODRIGUES and MARTA [14] synchronously optimized twist and chord length distribution as well as airfoil shape with respect to aerodynamic and aeroacoustic performance.

There is no doubt that the acoustic model is an essential and challenging ingredient for any type of a combined acoustic and aerodynamic optimization. According to LOWSON [15] wind turbine sound prediction methods can be subdivided into three classes: (i) empirical single equation models using general design parameters of a turbine (ii) semi-analytical models which model sound source mechanisms and (iii) high fidelity computational aeroacoustic methods.

The objective of this contribution is a two-step acoustic and aerodynamic optimization of the full 3D blade geometry, here exemplary for a small horizontal axis wind turbine. The sub-models should be more advanced as compared to the literature. Thus we focus on a combination of refined blade element momentum (BEM) method and a combined ROZENBERG/AMIET trailing edge noise model. The detailed airfoil boundary layer data relevant for the acoustic source model are taken into account. The optimization, however, is still subdivided into two independent steps, (i) the airfoil optimization, and (ii) the optimization of the blade twist angle and chord

length distributions. This two-step approach is thought reducing the optimization time and should enable a separate assessment of the optimization potential in both steps. The optimization itself is based on an in-house evolutionary algorithm as developed recently for axial fans (BAMBERGER [16]) and tidal horizontal axis turbines (KAUFMANN [17]).

2. Sub-models and optimization methodology

2.1 Aerodynamic performance prediction

A widely used representation of aerodynamic wind turbine performance is shown in **Fig. 1** in terms of the non-dimensional power coefficient

$$C_P \equiv \frac{P_{sh}}{0.5\rho c_0^3 A} \quad (1)$$

as a function of tip-speed ratio

$$\lambda \equiv \frac{U_{tip}}{c_0} . \quad (2)$$

A is the area swept by the rotor and c_0 the speed of the incoming wind far upstream of the turbine.

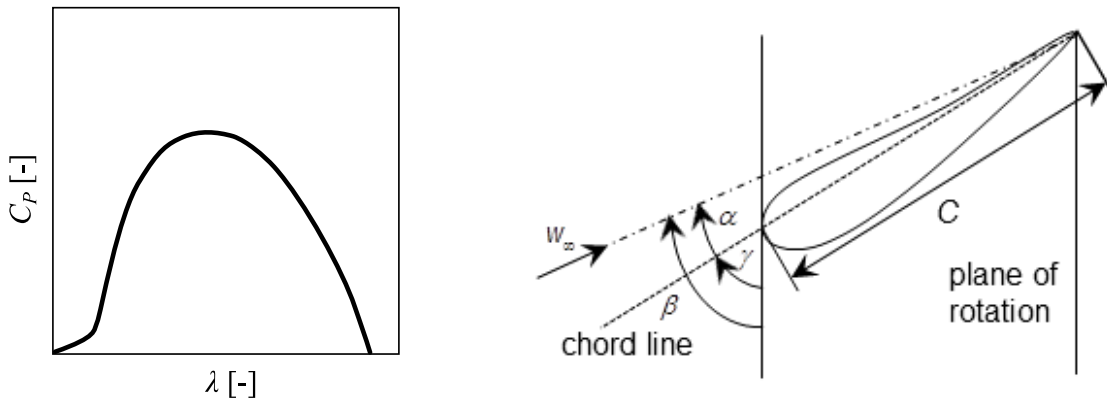


Fig. 1: Non-dimensional aerodynamic turbine characteristic (power coefficient as a function of tip-speed ratio) and relevant quantities at blade element (schematically)

Here we apply an enhanced in-house blade element momentum (BEM) method for performance prediction of a given wind turbine as described by KAUFMANN et al. [18]. In the context of this paper it is relevant, that within the BEM each blade is segmented along its span into a number of blade elements (BE), and that the inflow velocity w_∞ , the angle of attack α (see **Fig. 1**) and the local Reynolds number are known at each BE. The local aerodynamic forces on a BE can be used to calculate the power coefficient over all BE by evaluating the local circumferential force δF_u acting on each BE.

$$C_p(\lambda) \equiv \frac{\sum_{all\ BE} \delta F_u r 2\pi / n}{0.5 \rho c_0^3 A} = \frac{\sum_{all\ BE} P_{sh, BE}}{0.5 \rho c_0^3 A} \quad (3)$$

n is the rotational speed of the turbine and ρ the fluid density. The lift coefficient C_L of an airfoil can be calculated by the lift force F_L acting on each BE.

$$C_L \equiv \frac{F_L}{0.5 \rho w_\infty^2} \quad (4)$$

and local lift to drag ratio

$$\varepsilon \equiv \frac{F_L}{F_D} \quad (5)$$

are determined utilizing the public domain tool XFOil [4]. Hereby incompressibility is assumed as the Mach number is well below 0.3 for all BEs. In addition, to mimic a fully turbulent flow around the blades of a realistic wind turbine - a worst case scenario - tripping is applied at 2% and 5% of the BE chord length on suction and pressure side, respectively (unless specified otherwise).

2.2 Aeroacoustic performance prediction

For the prediction of the aeroacoustic performance we follow TIAN et al. [3], however with some extensions and modifications. Only trailing edge noise is taken into account. The BE is considered to be stationary (i.e. non-rotating) in a flow approaching the BE with w_∞ . **Fig. 2** depicts the work flow.

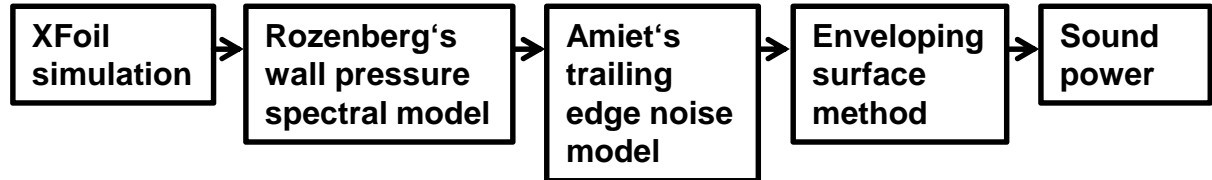


Fig. 2: Flow diagram of acoustic prediction model

On top of lift and drag XFOil yields BE boundary layer parameters which are essential input parameters in ROZENBERG's semi-empirical model (ROZENBERG et al. [5]) for the wall pressure spectrum beneath a turbulent boundary layer. According to ROZENBERG the normalized power spectral density of the wall pressure fluctuations at a given chordwise position is

$$\frac{\Phi_{pp}(\tilde{\omega}) w_e}{\tau^2 \delta^*} = \frac{\left[2.82 \Delta^2 (6.13 \Delta^{-0.75} + F_1)^{A1} \right] \left[4.2 \left(\frac{\Pi}{\Delta} \right) + 1 \right] \tilde{\omega}^2}{\left[4.76 \tilde{\omega}^{0.75} + F_1 \right]^{A1} + \left[8.8 R_T^{-0.57} \tilde{\omega} \right]^{A2}} \quad (6)$$

The normalized frequency, i.e. the Strouhal number, is

$$\tilde{\omega} = \omega \delta / w_e \quad (7)$$

with $\omega = 2\pi f$ being the angular frequency. The fluctuations are normalized with the free stream velocity w_e just outside of the boundary layer and a characteristic shear stress τ in the boundary layer. ROZENBERG sets τ as the maximum of the shear stress in the complete boundary layer. The earlier and well known wall pressure spectral model by GOODY [19] and more recent ones by KAMRUZZAMAN et al. [20] and CATLETT et al. [21] use the *wall* shear stress instead. In the current implementation we also use the wall shear stress which is easily obtained via the skin friction coefficient C_f from Xfoil¹

$$\tau_w = C_f \cdot 0.5 \rho w_\infty^2 \quad (8)$$

δ^* is the boundary layer displacement thickness. Furthermore, the ZAGAROLA-SMITS' parameter $\Delta = \delta / \delta^*$, COLE's wake strength parameter Π and CLAUSER's equilibrium parameter $\beta_c = (\theta / \tau_w)(dp/dx)$ - see for instance WHITE [22] - are needed. δ and θ are the boundary layer and momentum thickness, respectively, $R_T = 0.5 \cdot C_f Re \cdot (\delta / C)$ is the ratio of the outer to inner boundary layer timescale. Additional abbreviations are $A_1 = 3.7 + 1.5\beta_c$ and $F_1 = 4.76(1.4/\Delta)^{0.75}(0.375A_1 - 1)$. The parameter A_2 is set to 7, differently to ROZENBERG's suggestion, in order to limit the decrease of the wall pressure fluctuations at high frequencies to $\tilde{\omega}^{-5}$ as suggested by ROGER and MOREAU [23] and SANJOSE [24]. The boundary layer thickness is calculated as in DRELA and GILES [25]. It is convenient for the optimization of the airfoil contour to define a new non-dimensional wall pressure spectrum

$$\tilde{\Phi}_{pp}(\tilde{\omega}) \equiv \frac{\Phi_{pp}(\tilde{\omega}) w_\infty}{\left(\frac{1}{2} \rho w_\infty^2\right)^2 C} = \frac{C_f^2 \left(\frac{\delta^*}{C}\right) \left[2.82 \Delta^2 (6.13 \Delta^{-0.75} + F_1)^{A_1}\right] \left[4.2 \left(\frac{\Pi}{\Delta}\right) + 1\right] \tilde{\omega}^2}{\frac{w_e}{w_\infty} \left[4.76 \tilde{\omega}^{0.75} + F_1\right]^{A_1} + \left[8.8 R_T^{-0.57} \tilde{\omega}\right]^{A_2}}, \quad (9)$$

which is normalized with parameters w_∞ and chord length C , given and fixed during an optimization of the airfoil contour (but not necessarily during optimization of the complete blade shape). Integration of $\tilde{\Phi}_{pp}(\tilde{\omega})$ over $\tilde{\omega}$ yields the total power of the wall pressure fluctuations

$$P_{\tilde{\Phi}_{pp}} = \int_{\tilde{\omega}_1}^{\tilde{\omega}_2} \tilde{\Phi}_{pp}(\tilde{\omega}, \alpha) d\tilde{\omega} \quad (10)$$

The computed wall pressure spectrum is then used as an input for AMIET's trailing edge noise model [6]. The trailing edge is equivalent to the x_2 -axis in spanwise direction; x_1 is the chordwise coordinate and x_3 the direction perpendicular to the airfoil surface; the origin of the coordinate system is at mid span, **Fig. 3**.

¹ Throughout this study the Xfoil parameters are set as follows: $N_{crit} = 9$, $M = 0$ (incompressible), tripping at 2% and 5% on suction and pressure side, respectively.

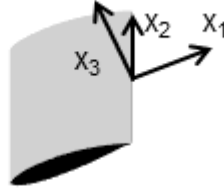


Fig. 3: BE and co-ordinate system; origin at mid span at the trailing edge

ROGER and MOREAU [7] added back scattering at the leading edge and a 3D extension to AMIET's model. Both extensions and the simplified model equation for large aspect ratios are used. The spectral density of the acoustic far field sound pressure is

$$S_{pp}(\mathbf{x}, \omega) = \left(\frac{x_3}{S_0} \right)^2 \left(\frac{\omega C}{4\pi c_s} \right)^2 2\pi L \left| I \left(\frac{K}{C}, \frac{kx_2}{CS_0}, \kappa \right) \right|^2 \frac{1}{\pi} \Phi_{pp} l_y \quad (11)$$

with the speed of sound c_s , the observer distance corrected for convection effects

$$S_0 = \sqrt{x_1^2 + (1 - M^2)(x_2^2 + x_3^2)} \quad (12)$$

the chord length C , the span of the blade element L , the wall pressure spectrum Φ_{pp} and the spanwise correlation length l_y . The spanwise correlation length l_y is calculated as in TIAN et al. [3] with the help of CORCOS' model [26]. The airfoil response function I is among others dependent on the acoustic wave number $k = \omega/c_s$ and the convective wave number $K = \omega/U_c$ with U_c being the convection velocity. Also super- and subcritical gusts are included which occur for $\kappa^2 > 0$ and $\kappa^2 < 0$, respectively, where

$$\kappa^2 = \left(\frac{KM}{1 - M^2} \right)^2 - \frac{K_2^2}{1 - M^2} \quad (13)$$

and the free stream Mach number $M = w_\infty/c_s$. As the large aspect ratio assumption is applied, the aerodynamic wave number in spanwise direction is $K_2 = kx_2/S_0$.

Eventually, the spectral far field sound power density is calculated on a spherical surface enveloping the BE. The radiation of the spectral density of the acoustic far field sound pressure calculated by eq. (11) is depicted in **Fig. 4**. The geometry and flow parameters of the S834 case which are described in the appendix are used for the calculation.

Integration over the surface area of the sphere yields the sound power spectral density emitted by a BE

$$S_{P, BE}(\omega) = \int_{A_{sp}} \frac{S_{pp}(\mathbf{x}, \omega)}{\rho_0 c_s} dA \quad (14)$$

with $\rho_0 c_s$ being the characteristic impedance of the acoustic medium.

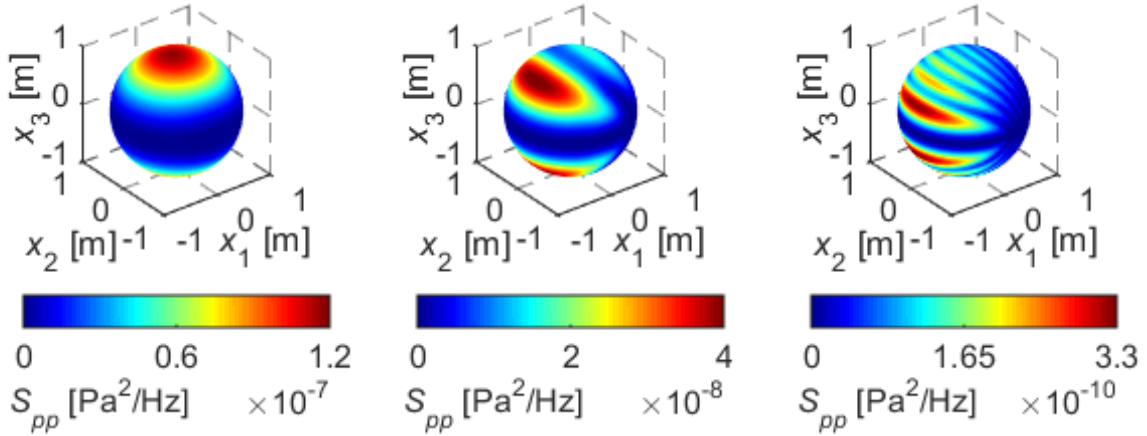


Fig. 4: Calculated spectral density of the acoustic far field sound pressure for different frequencies on a sphere as enveloping surface; frequency: $f = c_s / (C / 4)$ (left), $f = c_s / (C)$ (middle), $f = c_s / (4C)$ (right); values from the example in the appendix, note the different colour scales

A second integration over frequency from ω_1 to ω_2 results in the overall sound power or sound power level of a BE

$$P_{BE} = \int_{\omega_1}^{\omega_2} S_{P, BE}(\omega) d\omega, \quad LP_{BE} = 10 \log_{10} (P_{BE} / P_{ref}). \quad (15a, b)$$

Finally, the overall sound power level *OSWL* of the complete wind turbine is obtained by summation of the contributions from all n_{BE} BEs, the z blades and division by the reference sound power:

$$OSPL = 10 \log_{10} \left(2z \sum_{i=1}^{n_{BE}} (P_{BE,i}) / P_{ref} \right) \quad (16)$$

($P_{ref} = 10^{-12}$ W) with z being the number of blades. The factor 2 accounts for suction and pressure side, a conservative estimate, since the pressure side may contribute less as compared to the suction side. It has to be mentioned that neither an effect of the geometrical airfoil camber on the airfoil's radiation (ROGER and MOREAU [23]) nor the Doppler effect is considered as both do not change the radiated sound power.

2.3 Optimization

Optimization is done in two steps. Firstly, we seek an airfoil contour which provides maximum lift-to-drag-ratio at minimum trailing edge sound of a stationary BE. The trailing edge sound is due to the wall pressure fluctuations; hence, we minimize the wall pressure fluctuations rather the sound. As a representative location on the blade we take a monitoring point close to the trailing edge, here 90% of C . In a second step

the 3D blade shape, described by the distributions of chord length and twist angle, is optimized for high power coefficient and low overall sound power level.

Optimization of 2D airfoil contour. A design Reynolds number and a range of flow angles of attack are set for airfoil optimization. The airfoil geometry is parameterized utilizing Bezier curves. In total two times seven Bezier points are used to define upper and lower side of the airfoil for the upper and lower airfoil side as in KAUFMANN [17]. This is depicted in **Fig. 5**. During optimization the y -coordinates of ten Bezier points can be varied. The two leading and two trailing edge Bezier points are fixed. The trailing edge thickness is fixed to 0.2 % of the chord length.

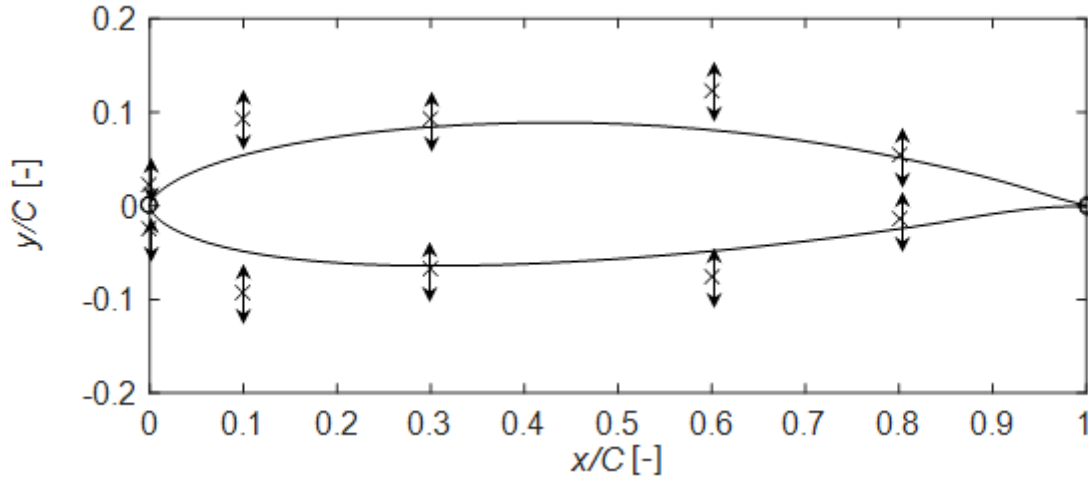


Fig. 5: Bezier points describing the airfoil geometry; the leading edge and the two trailing edge Bezier points denoted with circular markers are fixed

The objectives used for the airfoil optimization are listed in **Tab. 1**.

Tab. 1: Objectives for 2D airfoil optimization

Objective	Definition	α_{range}
Lift-to-drag-ratio	$\mathcal{E}_{obj} = \text{mean}(\mathcal{E}(\alpha_{range}))$	$0^\circ - 7^\circ$
Non-dimensional wall pressure fluctuations	$P_{\tilde{\phi}_{pp,obj}} = \text{mean}(P_{\tilde{\phi}_{pp}}(\alpha_{range}))$	$2^\circ - 6^\circ$

An airfoil with good aerodynamics for wind turbine applications offers a high lift-to-drag-ratio \mathcal{E} . \mathcal{E}_{obj} is the arithmetical mean of the lift-to-drag-ratio in a range of angles of attack $\alpha_{range} = 0^\circ - 7^\circ$ to safely avoid stall just outside of the targeted range of $2^\circ - 6^\circ$. The non-dimensional wall pressure spectrum $\tilde{\phi}_{pp}$, obtained by eq. (9), is integrated over a Strouhal range $0.05 \leq \tilde{\omega} \leq 10$ as described in eq. (10) - this is approximately the Strouhal range of the database ROZENBERG et al. [5] have built the model on and covers the maximum of the spectra. The wall pressure fluctuations are minimized for the targeted range of angles of attack $\alpha_{range} = 2^\circ - 6^\circ$. The two objectives are combined into the objective function

$$f_{obj,2D}(\mathbf{x}_{Bez,2D}) = \mathcal{E}_{obj} - g_\phi P_{\tilde{\phi}_{pp,obj}} - \sum_i^{n_{2D,PT}} g_{2D,i} PT_{2D,i}. \quad (17)$$

$PT_{2D,i}$ are penalty terms which are weighted by weighing factors $g_{2D,i}$. The $n_{2D,PT} = 5$ penalty terms are formulated such that

- the thickness of the airfoil increases monotonically from leading edge to the maximum thickness and then decreases monotonically towards the trailing edge of the airfoil
- extremely thin airfoils close to the trailing edge are avoided
- negative wall shear stress and hence flow separation along the chord are avoided
- a decrease of lift below a set limit is avoided
- contours yielding favourable pressure gradients at the monitoring point 90% C are disregarded since then the ROZENBERG model is invalid.

For $P_{\phi_{pp,obj}}$ the weighing factor is $g_{\phi} = g_{w,2D}g_{s,2D}$. With $g_{s,2D}$ the order of magnitudes of both, ϵ_{obj} and $P_{\phi_{pp,obj}}$ are adjusted to similar levels. With $g_{w,2D}$ the focus of the optimization on either lift-to-drag or wall pressure fluctuations is controlled.

Optimization of 3D blade shape. Starting point is the selection of a design operating point of the wind turbine in terms of tip speed ratio λ (eq. (2)) and the specification of the inflow velocity c_0 far upstream of the turbine.

The distributions of twist angle γ (**Fig. 1**) and chord length C are again defined by Bezier curves. Both distributions are parameterized with four Bezier points each as described by KAUFMANN [17] and depicted in **Fig. 6**. Their position in spanwise direction is fixed while γ and C is varied at those positions during optimization. Hence, the parameter space comprises eight parameters for the blade optimization.

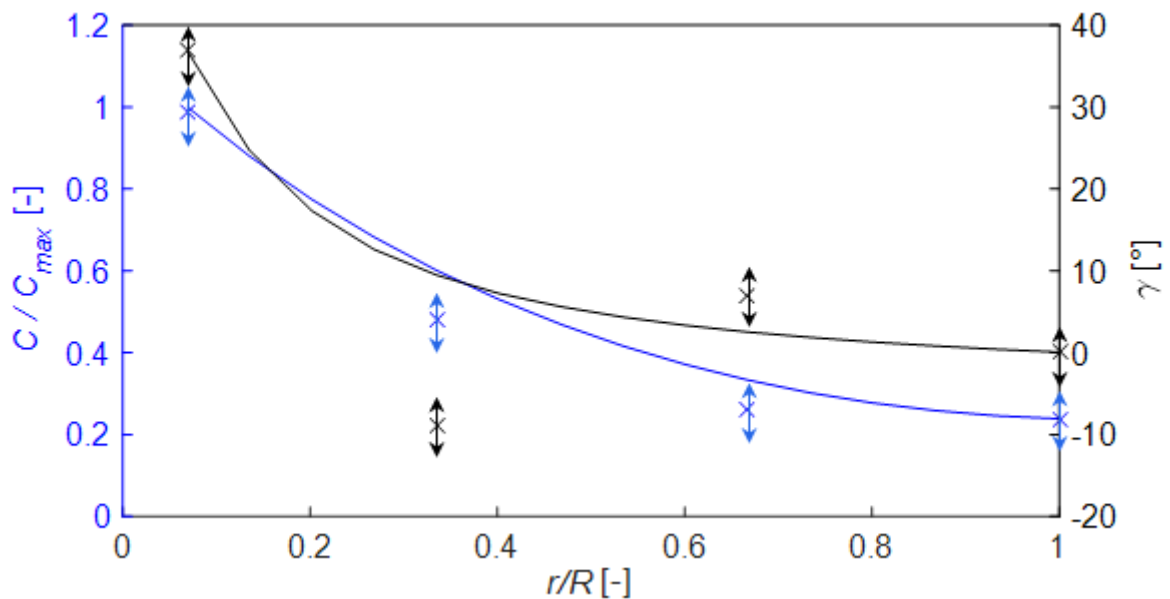


Fig. 6: Bezier points describing the blade distributions of chord length and twist angle

Eventually, with λ , c_0 , a given set of airfoils and the distributions of γ and C the turbine's overall sound power and power coefficient can be evaluated. Airfoil data, consisting of lift and drag coefficient and boundary layer information, for the local Reynolds number and angle of attack at each BE is needed for these evaluations. Instead of performing costly XFOIL calculations during the blade optimization, these airfoil data are prior to optimization calculated by XFOIL for a range of angles of attack and Reynolds numbers. These calculation results then form a characteristic map for

each parameter. These maps then are used for interpolating each parameter for the actual Reynolds number and angle of attack of each BE as utilized by KAUFMANN [17].

The objective function comprises the objectives power coefficient according to eq. (3) and the overall turbine sound power level *OSPL* according to eq. (16):

$$f_{obj,3D}(\mathbf{x}_{Bez,3D}) = g_c C_P - OSPL - \sum_i^{n_{3D,PT}} g_{3D,i} PT_{3D,i} \quad (18)$$

The $n_{3D,PT} = 2$ penalty terms are weighted by the weighing factors $g_{3D,i}$ and formulated such that

- the chord length at the hub of a turbine blade is short enough to avoid overlapping with one of the adjacent blades
- zero or negative wall shear stress and hence flow separation on the BEs is avoided.

For C_P the weighing factor is $g_c = g_{w,3D} g_{s,3D}$. With $g_{s,3D}$ the order of magnitudes of both, C_P and *OSPL* are adjusted to similar levels. With $g_{w,3D}$ the focus of the optimization on either the power coefficient or the overall sound power level is controlled.

2.4 Optimization algorithm and settings

The optimization algorithm employed is an evolutionary algorithm which is described by BAMBERGER [16]. The population sizes are 500 and 200 individuals for airfoil optimization and blade optimization, respectively. Crossover between the parent parameters, i.e. Bezier points, followed by mutation is applied to produce the individuals of the next generation. The mutation range producing the following generation is confined to 50% of the difference between the lowest and highest magnitude of the respective parameter in the previous generation. Only the best individual, the elite, will survive and be transferred to the next generation. Crossover is only performed within the first 40 generations. Convergence is reached if the Bezier points of the best individual vary less than 0.1% of the difference of the initial parameter limits within the last 40 generations.

3. Results

3.1 Benchmark turbine

The University of Siegen operates a small horizontal axis wind turbine USI S83x with 3 m rotor diameter. It was designed utilizing an early in-house design code where the standard blade element momentum method according to GLAUERT and SCHMITZ (i.e. no optimization) is encoded. The design inflow velocity was $c_0 = 6$ m/s and the design tip speed ratio $\lambda = 7.5$. The well-known family of SOMERS airfoil sections S835, S833 and S834 (from hub to tip) has been used to build up each of the three blades. More details are described by GERHARD et al. in [27].

This turbine will serve as a benchmark for the next steps. Therefore, its geometry was used as a first input in the aerodynamic and aeroacoustic performance prediction model eqs. (1) to (16). For that the blade was segmented in 15 BEs. The resulting spanwise distributions of two exemplary quantities are depicted in **Fig. 7**:

The angle of attack - in average it coincides well with the 5° chosen in the initial design -, and the Reynolds number.

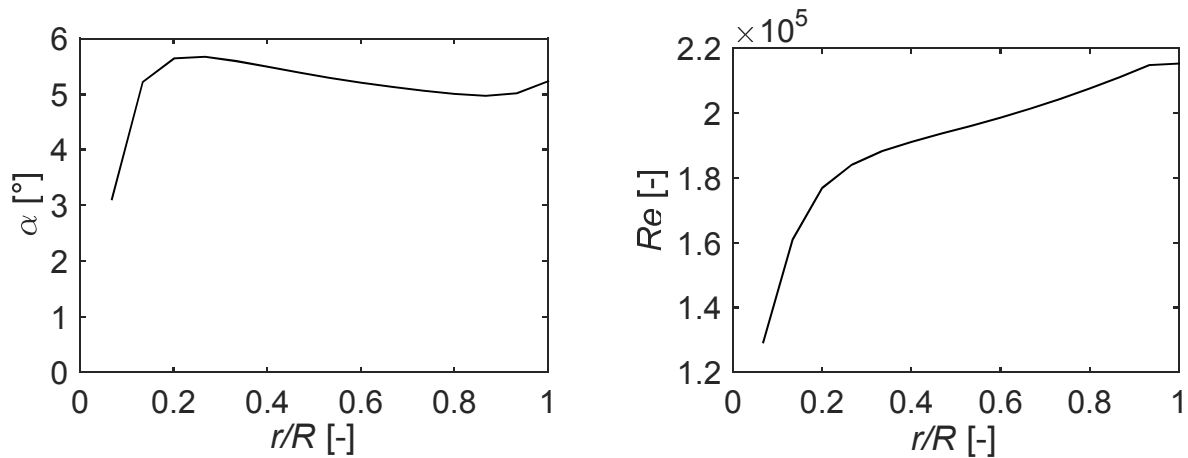


Fig. 7: Benchmark turbine: Predicted spanwise distribution of angle of attack (left) and Reynolds number (right)

Fig. 8 shows the shaft power $P_{sh, BE}$ each BE contributes, and the sound power emitted by each BE. On a trial basis, for the sound prediction the blade was also segmented into eight rather 15 BEs. As a consequence each BE is longer in spanwise direction and hence emits more sound power. But the value of overall sound power level $OSPL$ (with 15 BEs: 77.7 dB, with eight BEs: 77.5 dB) essentially remains constant as expected. The $OSPL$ is always evaluated within the frequency range 100 Hz to 10 kHz. It is obvious and expected that the inner BEs contribute very little to $OSPL$ - roughly speaking, the outer 30% of the blade determine the overall sound power level emitted by the turbine.

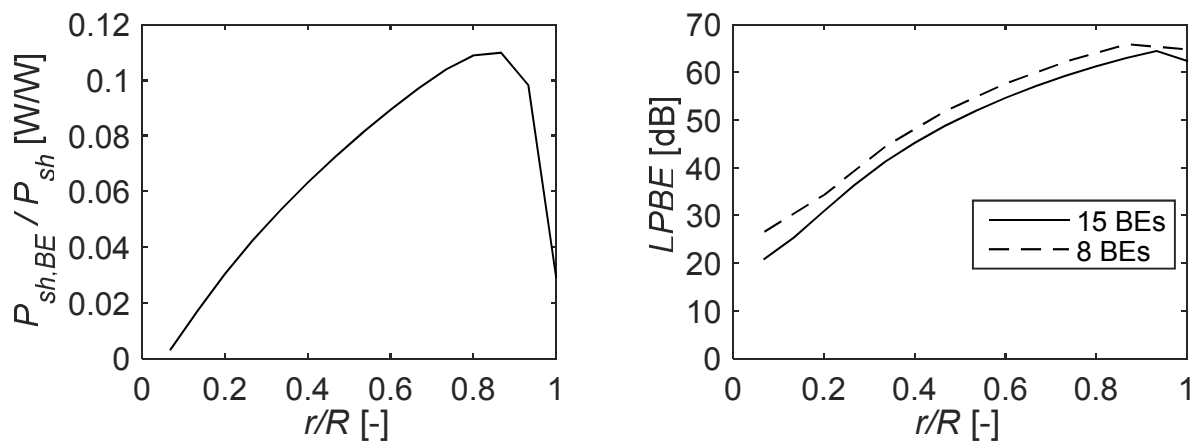


Fig. 8: Normalized spanwise distribution of shaft power from each of the 15 BEs (left); spanwise distribution of overall sound power level (right)

3.2 Optimization

As a potential replacement of the benchmark turbine we now seek an optimized turbine employing the optimization method introduced earlier. As already mentioned

optimization is done in two steps, firstly, airfoil optimization, secondly, the 3D blade shape while utilizing the optimized airfoil sections.

3.2.1 Airfoil optimization

The airfoil optimization algorithm is used to find airfoils for a design Reynolds number of 200,000 as for the benchmark turbine. Three different objectives for optimization have been chosen. The resulting airfoils are compiled in **Tab. 2**. Their corresponding lift-to-drag-ratio and the lift coefficient of all airfoils as a function of angle of attack (**Fig. 9**) are obtained utilizing XFOil, their non-dimensional WPS levels (**Fig. 10** and **Fig. 11**) by the aeroacoustic prediction method from section 2.2.

As targeted, both, KV100 and KV102 promise significantly lower non-dimensional WPS levels (more than 10 dB at a Reynolds number of 200,000) as compared to the benchmark airfoil S834. By contrast, KV101 performs at the highest lift-to-drag-ratio as expected, but KV100 is still superior to S834 with respect to lift-to-drag-ratio.

The aeroacoustic prediction method also allows studying the effect of angle of attack and Reynolds number on the near TE wall pressure spectrum WPS, cp. **Figs. 10** and **11**. As a conclusion the exclusively aerodynamically optimized airfoils S834 and KV101 are nearly insensitive to a variation of angle of attack and Reynolds number. By contrast, the acoustically optimized airfoils KV100 and KV102 gain from an increase of both, angle of attack and Reynolds number, at least in the range where the WPS model allows a prediction.

Comparing the lift-to-drag ratios of S834 and the new airfoils, one has to keep in mind that for all airfoils - as stated earlier - tripping was applied very close to the leading edge in order to mimic a fully turbulent boundary layer. Of course, a S834 airfoil with natural transition would have a substantially better lift-to-drag ratio. Finally, it is worth to note, that KV101 has two disadvantages: It is very thin, which may cause structural problems, and its lift polar deviates remarkably from the benchmark.

Tab. 2: Optimized airfoils and objectives

Airfoil	Objective for optimization
 <p style="text-align: center;">S834</p>	none, benchmark
 <p style="text-align: center;">KV100</p>	high lift-to-drag-ratio and minimal wall pressure fluctuation near TE
 <p style="text-align: center;">KV101</p>	high lift-to-drag-ratio
 <p style="text-align: center;">KV102</p>	minimal wall pressure fluctuation near TE

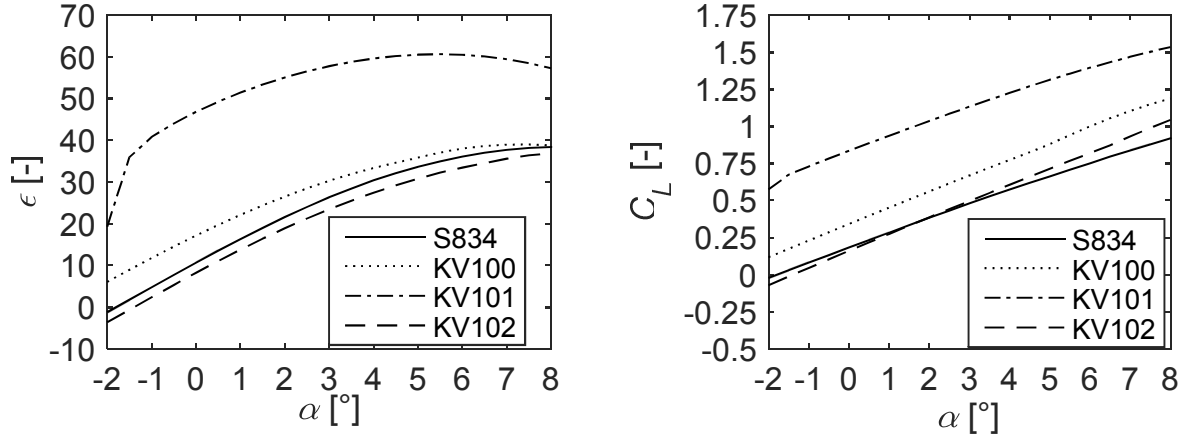


Fig. 9: Lift-to-drag-ratio (left) and lift coefficient (right) of the benchmark and the optimized airfoils; $Re = 200,000$

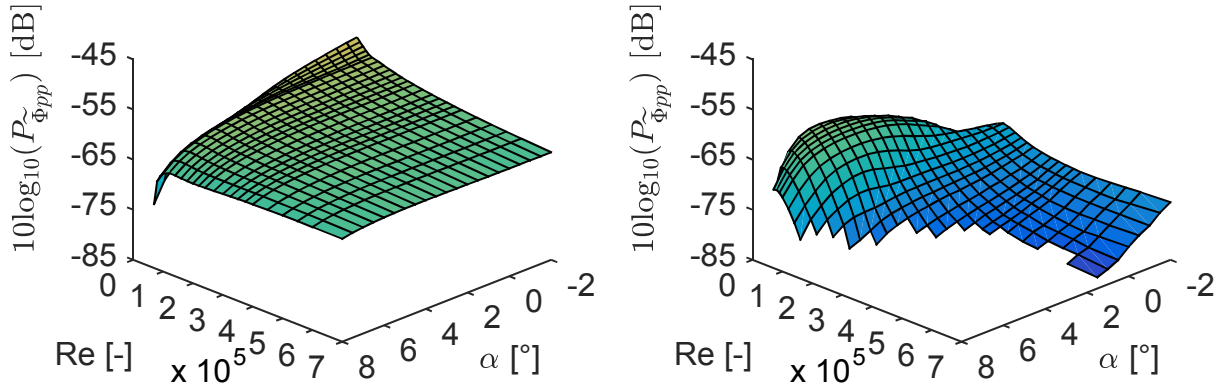


Fig. 10: Power level of the non-dimensional wall pressure fluctuations (eq. (10)) at 90% C; left: S834; right: KV100

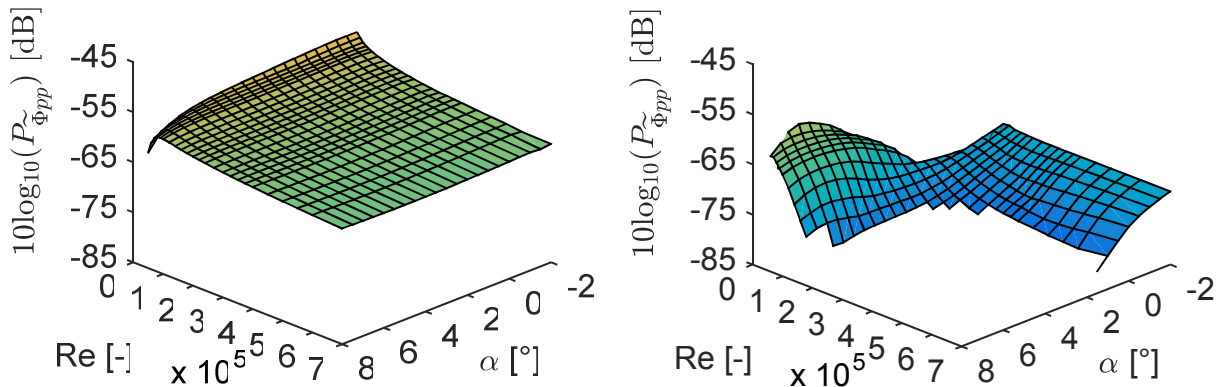


Fig. 11: Power level of the non-dimensional wall pressure fluctuations (eq. (10)) at 90% C; left: KV101; right: KV102

In **Tab. 3** most of the boundary layer parameters needed for the WPS calculation in eq. (9) are listed for an exemplary $\alpha = 5^\circ$ and $Re = 200,000$. In addition, the bounds of the empirical database as utilized by ROZENBERG et al. [5] for each parameter are given. ROZENBERG proposed the Reynolds number based on the mo-

momentum thickness Re_θ as an important parameter. It can be seen that Re_θ for all airfoils is inside of the bounds. Further examination reveals that for the airfoils S834 and the high lift-to-drag-ratio airfoil KV101 all other parameters are within the database bounds. By contrast, the acoustically optimized airfoils KV100 and KV102 require some extrapolation. Hence, these both airfoils are examined in more detail: As listed, low non-dimensional WPS levels come along with low skin friction coefficients C_f . This coefficient is an important scaling parameter in the applied WPS model eq. (9) as it is even squared. To achieve these low skin frictions the boundary layer shape factor H is large and represents boundary layers which are on the verge of separation at the considered chordwise position. Therefore, also CLAUSER's parameter β_c is very large and outside the database bounds. In addition, the ratio δ^*/C shows that the boundary layer displacement thicknesses is comparatively large. The wake strength parameter Π is also outside from ROZENBERG's empirical database.

Tab. 3: Inner and outer boundary-layer variables of the presented airfoils at an flow angle of 5° at 90% of airfoil chord length on the suction side; the bounds of the database, which ROZENBERG based his model on, are also given for comparison; $Re = 200,000$

	$H = \delta^*/\theta$	$C_f \cdot 10^4$	β_c	Π	$Re_\theta = w_e \theta/\nu$	Δ	δ^*/C
Bounds of ROZENBERG's database	1.33 — 2.55	—	0.19 — 20.9	1.03 — 8.18	564 — 17170	2.23 — 6.39	—
S834	2.26	8.75	14.95	6.03	1364	3.00	0.016
KV100	3.39	0.41	38.59	40.67	2003	2.14	0.035
KV101	1.68	31.0	5.36	1.93	1253	4.37	0.009
KV102	3.51	0.30	60.50	47.90	1812	2.09	0.033

3.2.3 Blade optimization

The blade optimization algorithm is used to find optimal blades for turbines with the same design parameters as the benchmark turbine USI S83x (design inflow velocity $c_0 = 6$ m/s, design tip speed ratio $\lambda = 7.5$, 3 m rotor diameter). Prior to the optimization of spanwise chord length and twist angle (cp. **Fig. 1**), the airfoil sections are chosen according to **Tab. 4**. The objective function comprises both, C_P and $OSPL$, equally weighted.

Tab. 4: Optimized wind turbines and objectives

Wind turbine	Blade	Objective for optimization
USI S83x	S835, S833 and S834 (from hub to tip)	none; University of Siegen research turbine as described in section 3.1, benchmark
USI KV100	KV100	maximize C_P and minimize $OSPL$
USI KV101	KV101	maximize C_P and minimize $OSPL$
USI KV102	KV102	maximize C_P and minimize $OSPL$

Convergence towards a final geometry is mandatory for optimization results to be acceptable. This is given for all airfoil and blade geometries presented. Addition-

ally, it was checked whether the optimization results are reproducible: Several optimizations with same settings were repeated. The optimization results (i.e. geometries) yielded similar objective function values for each of the repeated optimizations. This indicates that the optimizations tend to find global optima. This is true for airfoil and blade optimization.

Tab. 5 lists the predicted overall performance of the benchmark and optimized turbines. The optimized turbine USI KV102 performs best in terms of sound power emitted. Its *OSPL* is surprising 16 dB less than the benchmark USI S83x. Its power coefficient C_P , however, is 1.5% smaller as compared to USI S83x. USI KV101 performs with the largest power coefficient but the sound emission is slightly increased. USI KV100 is a good compromise: C_P remains as for the benchmark but its *OSPL* some 13 dB less.

Tab. 5: Predicted overall performance of benchmark and optimized turbines

	USI S83x (benchmark)	USI KV100	USI KV101	USI KV102
C_P [-]	0.412	0.413 (+0.2%)	0.456 (+10.7%)	0.406 (-1.5%)
<i>OSPL</i> [dB]	77.7	64.3 (-13.4 dB)	79.7 (+2.0 dB)	61.2 (-16.5 dB)

The corresponding optimized spanwise distributions of twist angle and chord length are presented in **Fig. 12**. The large lift coefficient of airfoil KV101 leads to a reduction of the chord length along the whole span of blade USI KV101 as compared to the benchmark. Otherwise, optimization yields modifications mainly in the hub region. As already pointed out the outer BEs contribute most to the overall performance data of the turbine. Hence, the benefits achieved by optimization are more attributed to the airfoil than to the spanwise distribution.

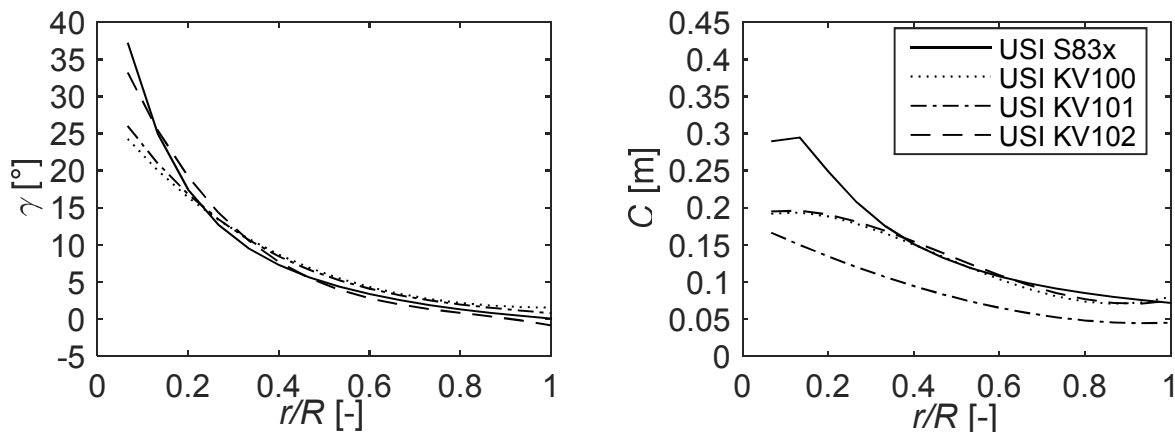


Fig. 12: Benchmark and optimized blades: Spanwise distribution of twist angle (left) and chord length (right) (cp Fig. 1)

It has to be emphasized again that the optimizer is bound to search for geometries only where the underlying models are valid. Utilizing XFOIL the chordwise region on the surfaces of each BE, where separation occurs, can be determined, called $C_{separated}$ as the sum from the pressure and suction side. An indicator is the skin friction coefficient with a value smaller than zero. **Fig. 13 (left)** shows a compar-

sion for all blades. Clearly, at all BEs with the new airfoil sections, the chordwise regions with separation is considerably smaller than for the S83x blade. Again, one has to keep in mind that tripping was applied very close to the leading edge. In general slight separation on the airfoil surface may not harm the quality of the AMIET-based sound prediction (STURM et al. [28]). Nevertheless, as a precaution, regions of separation were avoided by a penalty during airfoil and blade optimization.

Fig. 13 (right) shows the predicted significant reduction of the sound power emitted from each BE of the optimized turbines USI KV100 and USI KV102 as compared to USI S83x.

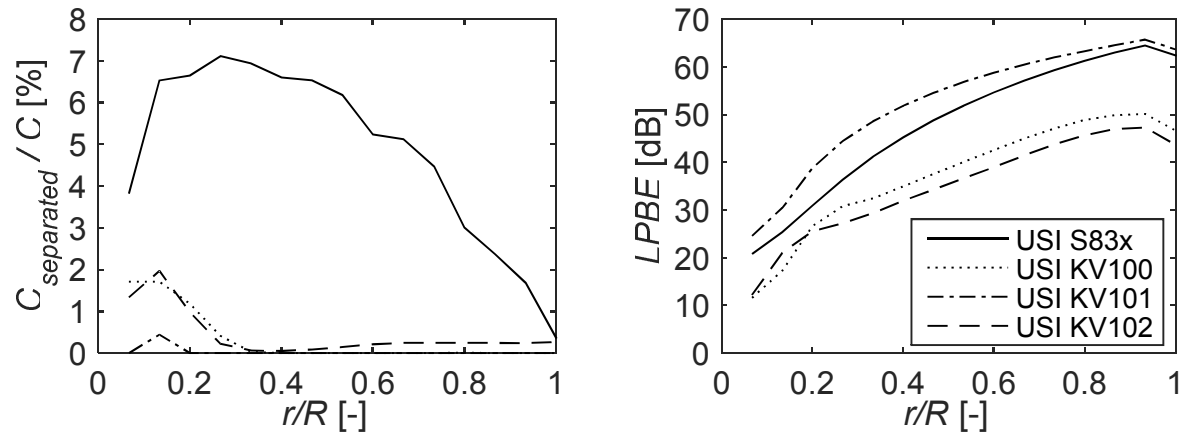


Fig. 13: Benchmark and optimized blades: Spanwise distribution of chordwise length of flow separation in per cent of chord length (left) and sound power emitted (right)

4. Summary and conclusions

Objective of this contribution was an acoustic and aerodynamic optimization of the full 3D blade geometry for a small horizontal axis wind turbine. Utilizing a refined aerodynamic blade element momentum (BEM) method and a combination of ROZENBERG's wall pressure and AMIET's trailing edge noise model (taking into account the adverse pressure gradient developing along a particular airfoil) an evolutionary algorithm was implemented. The optimization was subdivided into two independent steps, (i) the airfoil optimization, and (ii) the optimization of the blade twist angle and chord length distributions.

The validity of ROZENBERG and AMIET models was checked by comparison with recent own measurements of the wall pressure fluctuations and trailing edge sound of a small airfoil section. The agreement was satisfactory.

To mimic a fully turbulent flow around the blades of a realistic wind turbine - a worst case scenario - tripping was applied close to the leading edge of all airfoils. Depending on the set weighting in the objective function the airfoil optimization resulted in various novel airfoil shapes. As compared to a chosen reference airfoil S834 they promise better lift-to-drag-ratio and/or lower non-dimensional wall pressure fluctuations in the trailing edge region. The predictions forecast a possible reduction by more than 10 dB.

Utilizing such a low noise airfoil and optimizing spanwise chord length and twist angle distribution resulted in a new blade design. As compared to the non-

optimized benchmark turbine with SOMERS airfoil shaped blades the predicted sound power of a turbine equipped with the most feasible of these new blades is with -13 dB substantially lower, whereas the power coefficient remains constant. The detailed analysis leads to the conclusion that the sound reduction is mainly attributed to the improved airfoil sections.

Although the models implemented may not be very accurate in the complete range of parameters varied during optimization, the combined optimization of aerodynamic and acoustic performance seems to be a promising way for the design of low noise high performance wind turbines. In any case an experimental validation of the results achieved so far is indispensable.

Acknowledgment

The authors thank Julien Christophe from the von Kármán Institute for Fluid Dynamics in Sint-Genesius-Rode, Belgium for discussions regarding AMIET's theory and supplying a code with AMIET's trailing edge noise model. Additionally, the authors highly appreciate the assistance by Marlène Sanjose and Stéphane Moreau from the Université de Sherbrooke, Canada, especially for discussing the ROZENBERG model.

References

- [1] Gasch, R., Twele, J.: Wind power plants - Fundamentals, design, construction and operation. Berlin, Heidelberg, Springer, 2012
- [2] Leloudas, G.: Optimization of Wind Turbines with respect to Noise, Master Thesis, Technical University of Denmark, 2006
- [3] Tian, Y., Cotté, B., Chaigne, A.: Wind Turbine Noise Modelling Based on Amiet's Theory. 5th International Meeting on Wind Turbine Noise. 2013
- [4] Drela, M.: XFOIL: An Analysis and Design System for Low Reynolds Number Airfoils. In: Mueller, T. J. (Ed.): Low Reynolds Number Aerodynamics. Proceedings of the Conference Notre Dame, Indiana, USA, 5-7 June 1989. Lecture Notes in Engineering, Vols.54. Berlin, Heidelberg: Springer 1989, p. 1–12
- [5] Rozenberg, Y., Robert, G., Moreau, S.: Wall-Pressure Spectral Model Including the Adverse Pressure Gradient Effects. AIAA Journal Vol. 50 (2012) No. 10, p. 2168–2179
- [6] Amiet, R. K.: Noise due to turbulent flow past a trailing edge. Journal of Sound and Vibration Vol. 47 (1976) No. 3, p. 387–393
- [7] Roger, M., Moreau, S.: Back-scattering correction and further extensions of Amiet's trailing-edge noise model. Part 1 - Theory. Journal of Sound and Vibration Vol. 286 (2005) No. 3, p. 477–506
- [8] Amiet, R. K.: Acoustic radiation from an airfoil in a turbulent stream. Journal of Sound and Vibration Vol. 41 (1975) No. 4, p. 407–420
- [9] Schepers, J. G., Wuerz, W., Curvers, A., Mantesanz, A., Oerlemans S., Garcilán, L., Braun, K., Fischer, M., Lutz, T., Koenigler, K., Herrig, A., Maeder, T.: SI-ROCCO: Silent rotors by acoustic optimisation, ECN Energy research Centre of the Netherlands, 2007

- [10] Bertagnolio, F.: EUDP Project 'Low Noise Airfoil' - Final Report - DTU Wind Energy E-Report, DTU Wind Energy, Technical University of Denmark DTU Wind Energy-E-0004, Roskilde, Denmark
- [11] Göçmen, T., Özerdem, B.: Airfoil optimization for noise emission problem and aerodynamic performance criterion on small scale wind turbines. *Energy* Vol. 46 (2012) No. 1, p. 62–71
- [12] Brooks, T. F., Pope, D. S., Marcolini, M. A.: *Airfoil Self-Noise and Prediction*, NASA Reference Publication 1218 (Ed.), NASA Langley Research Center, 1989
- [13] Hao, X., Weimin, Z., Xiao, L., Jieping, L.: Aerodynamic and Aeroacoustic Optimization of Wind Turbine Blade by a Genetic Algorithm. 46th AIAA Aerospace Sciences Meeting and Exhibit
- [14] Rodrigues, S. S., Marta, A. C.: On addressing noise constraints in the design of wind turbine blades. *Structural and Multidisciplinary Optimization* Vol. 50 (2014) No. 3, p. 489–503
- [15] Lawson, M. V.: Assessment and Prediction of Wind Turbine Noise, Flow Solutions Report 92/19, ETSU W/13/00284/REP, pp. 1-59, 1992
- [16] Bamberger, K.: Aerodynamic Optimization of Low-Pressure Axial Fans. *Berichte aus der Strömungstechnik*, Ph.D. dissertation at the University of Siegen. Herzogenrath, Shaker, 2015
- [17] Kaufmann, N.: Optimierung des hydrodynamischen Entwurfs einer Gezeitenströmungsturbine, Diplomarbeit, Lehrstuhl für Strömungsmechanik und Strömungsmaschinen, Technische Universität Kaiserslautern, 2015
- [18] Kaufmann, N., Carolus, T., Starzmann, R.: An Enhanced and Validated Performance and Cavitation Prediction Model for Horizontal Axis Tidal Turbines - submitted to the *International Journal of Marine Energy*
- [19] Goody, M.: Empirical Spectral Model of Surface Pressure Fluctuations. *AIAA Journal* Vol. 42 (2004) No. 9, p. 1788–1794
- [20] Kamruzzaman, M., Bekiropoulos, D., Lutz, T., Würz, W., Krämer, E.: A semi-empirical surface pressure spectrum model for airfoil trailing-edge noise prediction. *International Journal of Aeroacoustics* Vol. 14 (2015) No. 5-6, p. 833–882
- [21] Catlett, M. R., Forest, J., Anderson, J. M., Stewart, D.: Empirical Spectral Model of Surface Pressure Fluctuations beneath Adverse Pressure Gradients. 20th AIAA/CEAS Aeroacoustics Conference. 2014
- [22] White, F. M.: *Viscous fluid flow*. McGraw-Hill series in mechanical engineering. New York, NY, McGraw-Hill Higher Education, 2006
- [23] Roger, M., Moreau, S.: Extensions and limitations of analytical airfoil broadband noise models. *International Journal of Aeroacoustics* Vol. 9 (2010) No. 3, p. 273–306
- [24] Sanjose, M.: Rozenberg's wall-pressure spectral model including the adverse pressure gradient effects, private communication, Siegen, Germany 2015
- [25] Drela, M., Giles, M. B.: Viscous-inviscid analysis of transonic and low Reynolds number airfoils. *AIAA Journal* Vol. 25 (1987) No. 10, p. 1347–1355
- [26] Corcos, G. M.: Resolution of Pressure in Turbulence. *The Journal of the Acoustical Society of America* Vol. 35 (1963) No. 2, p. 192–199
- [27] Gerhard, T., Sturm, M., Carolus, T. H.: Small Horizontal Axis Wind Turbine: Analytical Blade Design and Comparison With RANS-Prediction and First Experimental Data. *Proceedings of the ASME Turbo Expo 2013*

- [28] Sturm, M., Sanjose, M., Moreau, S., Carolus, T.: Application of Analytical Noise Models Using Numerical and Experimental Fan Data. 11th European Conference on Turbomachinery Fluid dynamics & Thermodynamics. ETC11, 2015
- [29] Gerhard, T.: Umströmte Tragflügelsegmente: Auswirkungen des Hinterkanten-ausblasens auf Strömungsgrenzschicht und Schallemission, Ph.D. dissertation at the University of Siegen. Aachen, Shaker Verlag, 2016

Appendix

A validation of the combined ROZENBERG/AMIET sub-model is given in this appendix. GERHARD [29] measured the sound of a SOMERS S834 airfoil section in an aeroacoustic wind tunnel. The Reynolds number $Re = w_\infty C / \nu$ was $3.5 \cdot 10^5$ and the effective angle of attack 4.7° . A special tripping was applied at 17% of the chord length on the suction side and at 76% on the pressure side. The chord length was 0.2 m and the span 0.266 m. The blade's suction side was instrumented with wall pressure sensors. The 90% position, i.e. a location close to trailing edge, is evaluated here. A "far field" microphone was placed at a reference position 0.3 m away from the trailing edge perpendicular to the incoming flow.

Fig. A presents a comparison of the near trailing edge wall pressure at 90% chord length

$$L_{\Phi_{pp}} = 10 \log_{10} \frac{\Phi_{pp}}{p_{ref}^2 / 1 \text{ Hz}} \text{ dB.} \quad (\text{A1})$$

and the acoustic "far field" spectra with

$$L_{Spp} = 10 \log_{10} \frac{\Phi_{pp}}{p_{ref}^2 / 1 \text{ Hz}} \text{ dB.} \quad (\text{A2})$$

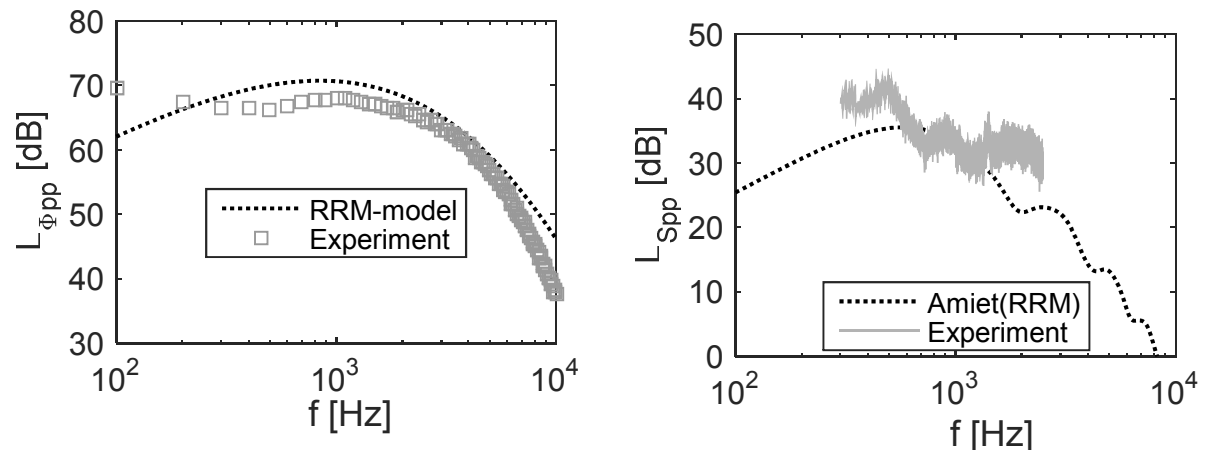


Fig. A: Left: Wall pressure spectral density at 90% chord length; right: "Far field" sound power spectral density at reference measuring position; reference pressure in both diagrams $p_{ref} = 2.5 \cdot 10^{-5}$ Pa; (ROZENBERG-ROBERT-MOREAU: RRM)

The acoustics at the reference position is calculated via AMIET's model fed with the wall pressure spectrum from the ROZENBERG model. Note that the input data for

the ROZENBERG model was obtained by XFOIL for exactly those transition points as enforced by the above mentioned tripping. Obviously, the agreement of the both, the wall pressure spectrum and the acoustic spectrum based on these data is satisfactory.